

Spectral Causality and the Scattering of Waves

Zeki Hayran, Aobo Chen, Francesco Monticone*

School of Electrical and Computer Engineering, Cornell University, Ithaca, New York 14853, USA

** Corresponding author: francesco.monticone@cornell.edu*

Classification: Physical Sciences - Engineering

Keywords: Metamaterials, photonics, time-varying systems, wave scattering, causality

Abstract – Causality – the principle stating that the output of a system cannot precede the input – is a universal property of nature. Here, we extend the concept of causality, and its implications, from the temporal to the spectral domain, leveraging the peculiar properties of time-modulated non-Hermitian wave-physics systems, with particular emphasis on photonic systems. Specifically, we uncover the existence of a broad class of complex time-modulated metamaterials which obey the time-domain equivalent of the well-established frequency-domain Kramers-Kronig relations. We find that, in the scattering response of such time-modulated systems, the output frequencies are inherently prohibited from spectrally preceding the input frequencies, hence we refer to these systems as ‘spectrally causal’. We explore the consequences of this newly introduced concept for several relevant applications, including broadband perfect absorption, temporal cloaking of an ‘event’, and truly unidirectional propagation along a synthetic dimension. By extending the concept of causality into the spectral domain and providing new tools to extend the field of temporally modulated metamaterials (“chrono-metamaterials”) into the complex realm, our findings not only deepen our understanding of spectral scattering dynamics, but may also open unexplored opportunities and enable relevant technological advances in various areas of photonics and, more broadly, of wave physics and engineering.

Significance Statement – The causality principle – an effect cannot temporally precede its cause – is a fundamental property of nature and underlies several constraints on the properties of physical materials. Here, we extend the notion of causality from the temporal to the spectral domain in temporally modulated wave-physics systems. Specifically, we uncover the existence of a broad class of time-modulated photonic systems that are “spectrally causal” in the sense that the output wave cannot contain oscillations with frequencies (colors) lower than the frequencies of the input wave oscillations. As an important consequence, wave reflections are then automatically minimized. This new class of time-modulated metamaterials has relevant implications for broadband perfect absorption, invisibility, unidirectional propagation, and may open unexplored opportunities in wave physics and engineering.

1. INTRODUCTION

In 1958, F. R. Morgenthaler noted that light experiences frequency scattering upon encountering a temporal perturbation [1], analogous to the occurrence of wavevector scattering when light impinges on a spatial perturbation. Although the field of temporal/frequency scattering has received comparatively less attention than its spatial/wavevector counterpart [2],[3], several subsequent studies have unveiled the rich physics embodied by wave propagation and scattering through time-varying media [4],[5],[6]. More recent studies on dynamical optical systems have further demonstrated the unique capabilities of such systems in several key areas, such as for optical isolation [7], delay-line buffering [8], topological phase transitions [9], among many others [10],[11],[12],[13], thereby renewing interest in this field. With a few exceptions discussed in the following [14],[15],[16],[17],[18], however, such systems have been investigated under the assumption that the temporal perturbation is essentially Hermitian (*i.e.* it does not involve the loss or gain properties of the system). However, to exploit all the degrees of freedom and the full capabilities of an electromagnetic/photonic system, the extension of the relevant optical parameters to the complex domain is clearly essential, both in the context of conventional absorption/emission and gain processes, and for more exotic phenomena involving exceptional points [19]. For instance, in the context of spatial scattering, parity-time (PT-) symmetric [20] or generalized non-Hermitian spatially modulated [21],[22] systems have been shown to exhibit many optical effects that are unattainable or difficult to achieve with their Hermitian counterparts, including unidirectional invisibility [23], exceptional-point based sensing and lasing [19], among others [20].

Temporally modulated systems might naturally lead to time-varying loss or gain, even when the designed modulation only involves the “Hermitian properties” of the system, *e.g.*, the refractive index. For instance, this could be due to the opening of a radiation/absorption channel by the modulation, or direct energy pumping into or from the optical system as in the process of parametric amplification [14]. Instead, despite the unexplored potential of this research direction, only few studies [14],[15],[16],[17],[18] have focused on the effect of temporal non-Hermiticity, in which, for example, a refractive index modulation is deliberately accompanied by a specific modulation of the loss/gain coefficient. In these earlier studies, however, the modulations were strictly implemented under certain symmetry requirements, for example PT-symmetry as in Refs. [14],[15],[17]. Aside from leading to the stringent necessity of gain materials, such strict symmetry conditions may not be suitable in practical applications where more complicated (non-periodic and asymmetric) forms of modulation may be easier to implement.

Within this context, here we uncover the existence of a broader class of non-Hermitian temporal modulations based on more general symmetries and relations between the real and imaginary parts of the modulation function. Specifically, we focus on temporal modulations that satisfy certain integral relations that are the temporal equivalent of the well-established Kramers-Kronig relations, and, thereby, possess a ‘causal spectral response’, *i.e.* the output frequencies generated by the temporal scattering process do not spectrally precede the input frequencies. To demonstrate the potential of this idea, we then present several representative applications, where the proposed concept of ‘spectral causality’ can have far reaching implications for the design of novel photonic devices. We note that unlike PT-symmetry requirements, the temporal Kramers-Kronig relations that lie at the basis of the concept of spectral causality, do not involve such strict symmetry constraints as a perfectly balanced distribution of loss and gain; instead,

they provide a way to design the imaginary part of the temporal modulation from the real part, or vice versa, regardless of their specific symmetries, in order to achieve certain advanced functionalities (perfect broadband absorption, invisibility, etc.). Hence, the ideas put forward in this article lead to a broader class of dynamically modulated structures with predetermined scattering properties, and represent a new step toward the goal of rigorously extending the field of metamaterials into the temporal domain.

2. THEORY

Consider a generic electromagnetic wave propagating in a homogeneous medium whose optical properties are dynamically varied in time, as illustrated in Fig. 1(a). Without loss of generality, we neglect magnetization effects and assume here that the medium exhibits only an electric polarization in response to an applied electric field. The constitutive relation between the electric field \mathbf{E} and the electric displacement field \mathbf{D} in a medium with a time-varying electric susceptibility can be written as $\mathbf{D}(\mathbf{r}, t, \omega') = \epsilon_0 [\epsilon_s + \chi(t, \omega')] \mathbf{E}(\mathbf{r}, t, \omega')$, where $\chi(t, \omega')$ is the dispersive time-varying complex electric susceptibility, ϵ_s is the static and spatially-homogenous background relative permittivity, and ϵ_0 is the permittivity of free space. The function $\chi(t, \omega')$ can be interpreted as the ‘spectrogram’ of the susceptibility profile, namely, the spectrum of the material response, $\chi(\omega')$, as it varies with time t . Specifically, as illustrated in Fig. 1(d), here the variable t corresponds to the time axis over which the temporal modulation occurs, while the ω' -axis shows the frequency response of the susceptibility function (*i.e.* the frequency dispersion of the material) at any t -time instant. To be able to use this simplified representation of a time-modulated frequency-dispersive material, we assume that the temporal modulation occurs on a time scale larger than the response time of the material. In other words, we operate at steady-state with a time-harmonic wave of frequency ω' , and the material is then modulated in t -time on a time scale larger than the time it takes the material to approximately reach a new steady state. Hence, in this t - ω' domain, \mathbf{E} and \mathbf{D} can be approximately related by a simple multiplication operation, as also discussed in [24]. In addition, since we are considering the material response in ω' -frequency domain, the function $\chi(t, \omega')$ is complex, with the imaginary part corresponding to time-varying loss or gain. In the following, we first consider a non-dispersive material, such that $\chi(t, \omega') = \chi(t)$ (*i.e.*, an instantaneous time-varying material response $\chi(t, t') = \chi(t) \delta(t')$) and will then discuss the role of dispersion at the end of this section.

In the dispersionless case, the vector wave equation in such a time varying medium can be written as

$$\nabla \times \nabla \times \frac{\mathbf{E}}{\mu_0} + \frac{\partial^2 \mathbf{D}}{\partial t^2} = 0, \quad (1)$$

where μ_0 is the permeability of free space. Since a time-varying spatially homogeneous medium conserves the wavevector \mathbf{k} of a propagating wave, we write the electric field in the medium in plane-wave form:

$\mathbf{E}(\mathbf{r}, t) = \mathbf{E}(t) \exp(-i\mathbf{k}\mathbf{r})\mathbf{n}$, where \mathbf{n} is the polarization vector, while the temporal function $\mathbf{E}(t)$ needs to be determined. Using the wave equation, the constitutive relation, and $|\mathbf{k}| = \omega_i \sqrt{\mu_0 \varepsilon_0 \varepsilon_s}$, we find the differential equation that governs the time evolution of \mathbf{D} as

$$\left(\varepsilon_s \frac{d^2}{dt^2} + \varepsilon_s \omega_i^2 \right) \mathbf{D}(t) = -\chi(t) \frac{d^2 \mathbf{D}(t)}{dt^2}, \quad (2)$$

where ω_i is the “incident” frequency (namely, the initial steady-state ω' -frequency of the field in the material before the modulation starts). Here, we define the time-varying Green’s function for the operator on the left side of Eq. (2) as $G(t)$, leading to the following recursive expression for $\mathbf{D}(t)$,

$$\mathbf{D}(t) = D_0 e^{i\omega_i t} + \int d\tau G(t-\tau) \left(-\chi(\tau) \right) \frac{d^2 \mathbf{D}(\tau)}{d\tau^2}, \quad (3)$$

where D_0 is the incident amplitude of \mathbf{D} . Fourier transforming Eq. (3) (going from t -time domain to ω -frequency domain) and reformulating it in terms of a scattering series gives (see Supplementary Material, Chapter 1), we obtain

$$\tilde{D}^{(N)}(\omega) = 2\pi D_0 \delta(\omega - \omega_i) + \sum_{m=1}^N \tilde{D}_s^{(m)}(\omega), \quad (4)$$

with,

$$\tilde{D}_s^{(m)}(\omega) = \tilde{G}(\omega) \left[\left(\tilde{\chi} * \omega^2 \tilde{D}_s^{(m-1)} \right) (\omega) \right] \quad \text{for } m > 1, \quad (5)$$

$$\tilde{D}_s^{(1)}(\omega) = 2\pi \omega_i^2 D_0 \tilde{G}(\omega) \left[\left(\tilde{\chi} * \delta \right) (\omega - \omega_i) \right], \quad (6)$$

where the operator “*” denotes convolution. In the above series, $\tilde{D}_s^{(1)}(\omega)$ can be regarded as the temporal analogue of the first-order Born approximation in the theory of spatial scattering [25]. Notice that in the case of a time-independent $\chi(t) = \chi$ (*i.e.* in the absence of any temporal modulation), $\tilde{\chi}(\omega)$ becomes $\tilde{\chi}(\omega) = 2\pi\chi\delta(\omega)$, and the convolution simply results in $(\tilde{\chi} * \delta)(\omega - \omega_i) = 2\pi\chi\delta(\omega - \omega_i)$ in Eq. (6). Hence, no spectral change to the incident field is expected as a first order approximation. Moreover, upon investigating all higher-order terms of the scattering series, $\tilde{D}_s^{(m)}$ in Eq. (5), we see that the incident field does not experience any spectral change at all (since throughout the series the only convolution operation is with $\tilde{\chi}(\omega)$), which is expected due to linearity and time-invariance. On the other hand, if $\chi(t)$ becomes time-dependent, the convolution in Eq. (6) produces a term $\tilde{D}_s^{(1)}(\omega)$ that is no longer a delta function centered at ω_i . In other words, the time-varying susceptibility “couple” the incident frequency ω_i with different frequency components (*i.e.* it generates different frequencies) depending on the spectral content of $\tilde{\chi}(\omega)$. Notably, an arbitrary $\tilde{\chi}(\omega)$ can even couple the incident frequency with ‘negative’ frequencies, analogous to

the creation of negative wavevectors that propagate backwards in space in the context of spatial scattering. However, note that the notion of negative frequencies does not imply backward propagation in time, as this would obviously violate temporal causality. Instead, negative frequencies should be interpreted as phase-conjugated waves that propagate backwards in space, leading to the phenomenon of temporal reflection [26] (see Fig. 1(b)).

Notice that in the special case when $\tilde{\chi}(\omega < 0) = 0$, $\tilde{\chi}(\omega)$ cannot promote frequency down-conversion, thereby the generation of any lower (including negative) frequencies is prohibited at all orders (see Fig. 1(c)). This can be seen as the spectral analogue of the concept of temporal causality, which states that a causal transfer function $H(t)$, for which $H(t < 0) = 0$, applied to a generic input function $f(t)$, for which $f(t < t_0) = 0$, results in an output function $g(t) = (H * f)(t)$ for which $g(t < t_0) = 0$. In other words, the output of a causal system cannot temporally precede the input. By analogy, we thus refer to any spectral susceptibility profile that satisfies $\tilde{\chi}(\omega < 0) = 0$ as ‘*spectrally causal*’, implying that the scattered waves arising due to such a temporal modulation profile cannot have components at frequencies that spectrally precede the input frequencies.

Since, by definition, a spectrally causal $\tilde{\chi}(\omega)$ is asymmetric around the frequency-axis origin, the temporal profile $\chi(t)$ is necessarily complex due to the properties of Fourier transforms (recall that a complex temporal profile is allowed since we are considering the material response in ω' -frequency domain). Therefore, one can expect that loss and/or gain must accompany the temporal modulation profile $\chi(t)$ to ensure its spectral causality, similar to the implications of the well-established Kramers-Kronig relations for a temporally casual response function (the real and imaginary part of the Fourier transform of a causal square-integrable function are not independent, and their mutual dependence is expressed by Kramers-Kronig relations). We can formalize this analogy by using the analytical properties of the Fourier transform of the causal function $\tilde{\chi}(\omega)$, that is, $\chi(t)$, to derive relations, analogous to the standard Kramers-Kronig relations, between the real and imaginary parts of the desired temporal modulation profile.

In fact, by noting that a spectrally casual $\chi(t)$ is an analytic function in the upper complex time plane if $\tilde{\chi}(\omega)$ and $\chi(t)$ are square integrable on the real line (which is satisfied by considering a finite temporal modulation that vanishes at large times), we can derive integral relations for $\chi(t)$ that relate its real $\chi_{\text{re}}(t)$ and imaginary $\chi_{\text{im}}(t)$ parts using complex analysis [27]:

$$\chi_{\text{re}}(t) = -\frac{1}{\pi} \text{P} \int_{-\infty}^{\infty} dT \frac{\chi_{\text{im}}(T)}{t - T}, \quad (7)$$

$$\chi_{\text{im}}(t) = \frac{1}{\pi} \text{P} \int_{-\infty}^{\infty} dT \frac{\chi_{\text{re}}(T)}{t - T}, \quad (8)$$

where P indicates the Cauchy principal value of the integral. The form of Eqs. (7) and (8) differs from the conventional Kramers-Kronig relations by a minus sign (originating from the fact that the conventional Kramers-Kronig relations are based on analyticity in the *lower* complex frequency plane). Hence, we refer to them as the *anti-Kramers-Kronig relations* in time domain. Such relations are a key result of this work, as they allow us to choose the specific temporal modulation function of the real and imaginary part of the susceptibility (hence the temporal modulation of the refractive index and of the loss/gain coefficient) such that the modulation is spectrally causal and, therefore, it does not induce frequencies preceding the incident frequency. As discussed in the following, this is relevant for a plethora of applications.

A rather important point to stress here is that additional constraints must be applied on a physical susceptibility function $\chi(t, \omega')$ such that *temporal* causality is not violated. Particularly, the conventional Kramers-Kronig relations imply that (i) the complex ω' -frequency-domain susceptibility $\chi(t, \omega')$ of any physically realizable material is always dispersive, namely, it is not a constant with respect to the frequency ω' of a time-harmonic wave at any t -time instant, and (ii) frequency dispersion is intimately related to absorption/gain processes.

Hence, the above discussion for the case of spectral causality holds true and is physically realizable only if the following conditions are met (illustrated in Fig. 1(d)): (1) for every value of ω' that is being generated throughout the frequency scattering process, the condition $\tilde{\chi}(\omega < 0, \omega') = 0$ must be satisfied to ensure spectral causality; (2) at every t -time instant, $\chi(t, \omega')$ must satisfy the conventional Kramers-Kronig relations along the ω' -axis to ensure temporal causality (see Fig. 1(d)). As mentioned above, frequency dispersion is a manifestation of temporal causality and must be included in every polychromatic system to ensure its physical nature (all the full-wave simulations of time-varying systems in the next sections properly include frequency dispersion). We also note that in the PT-symmetric temporal modulation in Ref. [16], material dispersion was not considered despite operating with large amplitudes of gain and loss around a wide frequency bandwidth, a situation that is, therefore, unphysical.

We conclude that a temporally modulated material susceptibility that satisfies both the anti-Kramers-Kronig relations (as in Eqs. (7) and (8)) in the t -time domain, at least for a certain ω' -bandwidth, and the conventional Kramers-Kronig relations in the ω' -frequency domain for all t -time instants, is spectrally casual and physically realizable (Fig. 1(d)). These conditions will ensure that an incoming wave only scatters to higher frequency components with no “back-scattering” to lower frequencies (including negative frequencies, corresponding to phase-conjugated and reflected waves). In addition, since the temporal part of \mathbf{D} is separated from its spatial part, the spectral causality property will be independent of the spatial properties of the incoming wave, such as polarization, beam-shape and propagation direction [28]. Also important to point out is that the anti-Kramers-Kronig relations are sufficient but not necessary to realize a reflectionless time-varying system. Indeed, purely Hermitian temporal profiles can also be found that are reflection-free [28,29], which, however, do not provide the same flexibility in terms of controlling the frequency scattering process, as further elucidated in the next sections.

3. APPLICATIONS

a. Broadband Reflectionless Spectrally Causal Absorbers

One immediate application to verify our theory is to design a spectrally casual absorber, which automatically prevents the coupling of the incident frequency to any negative frequencies and, therefore, eliminates any back-reflections and fully absorbs the incident wave, as illustrated in Fig. 2(a). To satisfy both the temporal anti-Kramers-Kronig relations and the conventional spectral Kramers-Kronig relations for such an absorbing medium, we propose the following material model,

$$\chi(t, \omega') = \frac{\omega_p^2}{(\omega_0 - K(t - t_{\text{offset}}))^2 - \omega'^2 + i\gamma\omega'}, \quad (9)$$

which is a standard Lorentz-type dispersion with plasma frequency ω_p , damping frequency γ , and with a time-varying resonance frequency $\omega'_0(t) = |\omega_0 - K(t - t_{\text{offset}})|$ (see lower right inset of Fig. 2(a)). Here, the parameter K determines the rate of change of the resonance frequency and t_{offset} provides a t -time offset. Eq. (9) is plotted on the (t, ω') plane in Figs. 2(b) and 2(c), for parameters given in the Methods section. It is apparent that Eq. (9) fully satisfies the conventional Kramers-Kronig relations along the ω' -frequency axis at any time instant t . Moreover, it also approximately satisfies the anti-Kramers-Kronig relations along the t -axis within a certain time window that can be chosen via t_{offset} (see Supplementary Material, Chapter 2). Note that this spectrally causal non-Hermitian temporal modulation only involves loss, while gain is not required.

Fig. 2(d) shows the spectral change of an incident broadband wave obtained through fully causal time-domain simulations (see Methods section). As expected, one can observe the absence of any reflections *at any frequency* (absence of standing wave behavior) and the frequency upshifting of the wave within the material. We stress here that since the material is physical and temporally causal, the wave experiences a different $\chi(t, \omega')$ profile as the frequency ω' upshifts. In other words, the temporal profile that the incident wave ultimately experiences is a synthesis of various $\chi(t, \omega')$ profiles determined by the frequency scattering process. However, since the material dispersion, Eq. (9), is designed to satisfy spectral causality also at these scattered higher frequencies (as shown in Figs. 2(b) and 2(c)), no lower frequencies (including negative frequencies) are generated throughout the propagation and scattering process. Hence, the wave will be fully absorbed within the medium without any back scattering, as seen in Fig. 2(d). Remarkably, the proposed theory still holds, and no reflection occurs, even though the temporal variation of $\chi(t, \omega')$ is relatively fast and non-adiabatic (the temporal linewidth of the Lorentzian loss profile in Fig. 2(c) is approximately equal to 3 fs, which is comparable to the period of the incoming wave). In other words, although our assumption that the temporal modulation is applied on a time scale much larger than the response time of the material may not be valid in this scenario, the qualitative predictions of our theory still hold even for relatively fast temporal variations. This

agrees with the recent findings in Ref. [30] that, even if the temporal variation is on a scale comparable to the period of the driving wave, one can still define a physically meaningful time-varying susceptibility $\chi(t, \omega')$. However, we note that more research is needed to understand the full ramifications of non-adiabaticity in the context of spectrally causal temporal modulations.

For comparison, a static structure with the same Lorentz dispersion as in Eq. (9) but without the temporal variation in ω_0 (i.e., $K = 0$) was also analyzed and the results are provided in Fig. 2(e). We see that despite the high losses in the medium, the wave is mostly backscattered rather than absorbed due to the high impedance mismatch resulting from the large amplitude of the Lorentzian profile. This is a rather striking result showing how a suitable spectrally causal temporal modulation can lead to *perfect broadband absorption* even when the corresponding static structure is largely impedance mismatched and almost perfectly reflective. Fig. 2(f) provides a further quantitative comparison between the reflected Poynting vector amplitude $|\mathbf{S}|$ (flow of energy per unit area per unit time) of the time-varying spectrally causal case and the time-invariant case. The difference between the reflected $|\mathbf{S}|$ and the input $|\mathbf{S}|$ quantifies the absorbed energy within the system, which confirms that, in contrast with the static structure, the designed dynamic medium absorbs nearly the entire broadband input radiation (see also Supplementary Movie 1^(†), which provides a detailed view into the broadband pulse propagation for both the dynamic and the static case). A rather important point worth mentioning is that reflectionless absorption over a broad bandwidth does not necessarily require the temporal modulation of the system parameters. As discussed in, for example, Refs. [31],[32],[33], broadband reflectionless absorption can be achieved in certain time-invariant and linear structures, such as reciprocal adiabatically tapered waveguides [31], or nonreciprocal (albeit time-invariant) terminated one-way waveguides [33]. Here, instead of adiabaticity or inherently unidirectional propagation, the lack of reflections is enabled by the spectral causality of the material (absence of scattered frequencies preceding the input frequency), thus enabling a potentially more compact and flexible system to achieve perfect broadband absorption, without the need for tapering or strictly unidirectional modes, and independently of the polarization, beam shape, and propagation direction of the incoming wave.

b. Temporal Cloaking of an ‘Event’

As mentioned above, an arbitrary time-varying $\chi(t, \omega')$ profile can induce frequency scattering, including back-reflected waves. An external observer will then be able to tell the existence of the time-varying $\chi(t, \omega')$ perturbation by simply detecting any scattered fields (see Fig. 3(a)). To illustrate this, Figs. 3(b) and 3(c) show, respectively, a refractive index perturbation and the temporally resolved field amplitude distribution propagating through a medium with such a perturbation. The reflections induced by the perturbation can be clearly seen in Fig. 3(c), in the form of fields propagating forward in t -time but in the backward spatial direction. In this regard, another intriguing application of the proposed concept of spectral causality would be to design a temporal ‘cloak’ that will reduce any back- and forward- scattered waves induced by a refractive index perturbation, restoring the incident wave after a certain t -time (analogous to spatial cloaks which restore the incident field after a certain *distance*), as shown in Fig. 3(d).

To get more insight into this process, we first consider a temporal profile $\chi(t, \omega')$ written as the sum of two identical generic profiles with different weight and temporal offset, $\chi(t, \omega') = f_1 \chi_0(t - t_{\text{offset},1}, \omega') + f_2 \chi_0(t - t_{\text{offset},2}, \omega')$. Fourier transforming $\chi(t, \omega')$ gives

$$\tilde{\chi}(\omega, \omega') = 2if_2 \tilde{\chi}_0(\omega, \omega') \sin\left(\omega \frac{t_{\text{offset},1} - t_{\text{offset},2}}{2}\right) \exp(-i\omega \frac{t_{\text{offset},1} + t_{\text{offset},2}}{2}) + (f_1 + f_2) \tilde{\chi}_0(\omega, \omega') \exp(-i\omega t_{\text{offset},1}). \quad (10)$$

We assume that $\tilde{\chi}_0(\omega, \omega')$ (and therefore $\tilde{\chi}(\omega, \omega')$) is spectrally causal within a certain t -time window (as in the Lorentz medium presented in the previous section). Here, we are especially interested in suppressing the forward and backward scattered waves at the same frequency ω_i of the incident wave. Different frequency components of the scattered field would not be able to propagate in the same medium after the modulation ends, as there would not be any allowed propagation modes at that frequency $\neq \omega_i$ and value of momentum (momentum of the propagating wave does not change since the system is spatially homogenous); these different frequency components would then be dissipated by any loss in the static system.

By referring back to Eq. (6) one notes that, as a first-order approximation, the forward- and backward-scattered waves at frequency $+\omega_i$ and $-\omega_i$, respectively, that is, $\tilde{D}_s^{(1)}(\pm\omega_i)$, are determined only by the values of the susceptibility function, $\tilde{\chi}(0, \omega')$ and $\tilde{\chi}(-2\omega_i, \omega')$, respectively (due to the convolution with $\delta(\omega - \omega_i)$). Thus, if these values (frequency components) vanish simultaneously in Eq. (10), the scattered waves $\tilde{D}_s^{(1)}(\pm\omega_i)$ will be suppressed completely. In this case, since any higher-order scattered term (see Eq. (5)) is directly related to the lower-order terms, the *complete* suppression at the first-order contribution will, in fact, also translate into zero scattering at all orders, i.e., $\tilde{D}_s^{(m)}(\pm\omega_i) = 0$, and hence lead to an invisibility effect at frequency ω_i . In Eq. (10), the condition $\tilde{\chi}(-2\omega_i, \omega') = 0$ is automatically satisfied because of the spectral causality of $\tilde{\chi}_0(\omega, \omega')$. However, note that $\tilde{\chi}_0(0, \omega') \neq 0$ since the considered temporal modulation profile is spectrally causal only within a certain t -time interval (due to this truncation, the integral $\tilde{\chi}_0(0, \omega') = \int \chi_0(t, \omega') dt$ will not vanish anymore). Thus, although the first term in Eq. (10) automatically vanishes for $\omega = 0$, the second term vanishes only if $f_1 = -f_2$, which can be satisfied through a time-varying medium with a balanced gain-loss profile. Following this insight, we employ the following dispersion model (see Methods section), to realize the cloaked refractive-index perturbation,

$$\chi(t, \omega') = \frac{f_1 \omega_p^2}{\left(\omega_0 - K(t - t_{\text{offset},1})\right)^2 - \omega'^2 + i\gamma\omega'} + \frac{-f_1 \omega_p^2}{\left(\omega_0 - K(t - t_{\text{offset},2})\right)^2 - \omega'^2 + i\gamma\omega'}. \quad (11)$$

The “temporal cloak” profile consisting of the temporal loss and gain modulation is shown in Fig. 3(e), while Fig. 3(f) shows the space-time evolution of the pulse propagating within the temporally cloaked medium (see also Supplementary Movie 2^(†) for a time animation compared with the uncloaked case). Note the absence of any back-

scattering from the perturbation (no fields propagating in the backward spatial direction), and the re-emergence of the absorbed wave after a certain t -time interval (this behavior can be considered the temporal equivalent of the PT-symmetric spatial cloaks studied in [23]). As the wave is reconstructed, additional scattered high-frequency components are still present in the system, which are, however, unable to propagate and are eventually absorbed, consistent with the discussion above (such spatially localized, temporally decaying fields can clearly be seen in Fig. 3(f)). Moreover, we note that the fields between the lossy and active space-time regions in Fig. 3(f) are not identically zero, such that the wave can be reconstructed through the amplification of these small fields. In other words, the system does not need prior knowledge about the incoming wave, but it naturally provides an ‘information channel’ between these two space-time regions that allows the automatic reconstruction of the wave through the concerted action of loss and gain (we acknowledge, however, that in practice this amplification and reconstruction process would certainly add some noise to any signal being transmitted).

To emphasize the importance of the role played by spectral causality, we have provided in Supplementary Movie 2^(†) an alternative case with balanced gain and loss where, however, the profile does not respect spectral causality. Although the gain and loss profile is identical as in the cloaked case, here the interplay between the real and the imaginary parts of the temporal modulation is broken (hence, Eq. (10) does not vanish for forward- and back-scattered waves). Thus, as seen in Supplementary Movie 2^(†), no cloaking effect occurs for such a non-causal profile, despite having a balanced gain-loss distribution.

The proposed cloaking scheme can be potentially useful for shielding information transfer from temporal perturbative effects (e.g. thermal or electrical fluctuations, mechanical movement/vibrations, etc.) that can affect the material properties of the medium, and the functionality of the system, as a function of time. We also stress here that, since the cloaking process requires gain materials, the stability of the system must be carefully analyzed to avoid any diverging oscillations [34],[35],[36]. A detailed stability analysis is beyond the scope of this paper. Nevertheless, we speculate that the proposed cloaking mechanism should be relatively robust against such instabilities. This is because no feedback mechanism exists that can lead to a resonance phenomenon (due to the absence of any back-scattered waves) and, unlike static active systems, the gain materials here are *temporally* localized, *i.e.* the gain process is not permanent, which may allow any unstable response to die out after optical gain is switched off. A detailed analysis of these effects will be the subject of future work.

c. Loss-Induced Unidirectional Transport Along a Synthetic Dimension

Another intriguing application of the proposed concept of spectral causality is related to wave ‘propagation’ along a synthetic dimension (see Fig. 4(a)). Such synthetic dimensions in photonic structures have recently become the subject of intense research, as they enable observing higher-dimensional physics in seemingly lower-dimensional systems [37]. Here, we theoretically demonstrate that spectral causality can lead to *truly one-way propagation* along a synthetic dimension defined by the sequence of resonant frequencies of a resonator, as illustrated in Fig. 4(a). Since different modes of a resonator do not contain the same momentum/wavevector components (spatial spectrum) [38], we revisit

our theory to include also momentum coupling between different modes. We re-write Eq. (1) with a time- and space-dependent $\chi(\mathbf{r}, t, \omega')$ as,

$$\nabla \times \nabla \times \frac{\mathbf{nE}}{\mu_0} + \mathbf{n} \frac{\partial^2 \varepsilon_s \mathbf{E}}{\partial t^2} = -\mathbf{n} \frac{\partial^2 \mathbf{P}}{\partial t^2}, \quad (12)$$

$$\mathbf{P}(\mathbf{r}, t, \omega') = \chi(\mathbf{r}, t, \omega') \mathbf{E}(\mathbf{r}, t, \omega'),$$

where \mathbf{P} is the polarization density generated by $\chi(\mathbf{r}, t, \omega')$. Decomposing the harmonic components of $\chi(\mathbf{r}, t, \omega')$ and assuming its temporal and spatial parts are separable gives,

$$\chi(\mathbf{r}, t, \omega') = \frac{1}{(2\pi)^2} \int d\mathbf{k} \tilde{\chi}(\mathbf{k}, \omega') e^{-i\mathbf{k}\mathbf{r}} \int d\omega \tilde{\chi}(\omega, \omega') e^{i\omega t}. \quad (13)$$

Then, we decompose \mathbf{E} in its frequency eigenmodes, each expanded into its spatial harmonic components, obtaining

$$\mathbf{E}(\mathbf{r}, t) = \frac{1}{2\pi} \sum_m c_m e^{i\omega_m t} \mathbf{E}_m(\mathbf{r}) = \frac{1}{2\pi} \sum_m c_m e^{i\omega_m t} \int d\mathbf{k} \tilde{\mathbf{E}}_m(\mathbf{k}) e^{-i\mathbf{k}\mathbf{r}}, \quad (14)$$

where c_m and ω_m are the amplitude and frequency of the m th mode, respectively. $\mathbf{E}_m(\mathbf{r})$ is the eigenmode spatial field profile that can be obtained by solving the eigenequation $\nabla \times \nabla \times \mathbf{nE}_m = \mu_0 \varepsilon_s \omega_m^2 \mathbf{nE}_m$. The induced \mathbf{P} for a specific mode m then becomes,

$$\mathbf{P}(\mathbf{r}, t, \omega') = \frac{c_m}{(2\pi)^3} \int d\mathbf{k} (\tilde{\mathbf{E}}_m(\mathbf{k}) * \tilde{\chi}(\mathbf{k}, \omega')) e^{-i\mathbf{k}\mathbf{r}} \int d\omega \tilde{\chi}(\omega, \omega') e^{i(\omega_m + \omega)t}. \quad (15)$$

Eq. (15) shows that a spatially homogeneous $\chi(\mathbf{r}, \omega')$ (hence, $\tilde{\chi}(\mathbf{k}, \omega') \propto \tilde{\chi}(\omega') \delta(\mathbf{k})$) cannot couple the different wavevector components of different modes (in other words, $\tilde{\chi}(\mathbf{k}, \omega')$ generates an induced polarization current with zero overlap integral with the field distribution of a different mode, resulting in zero coupling). One way to break the spatial symmetry is to apply the temporal modulation on an isolated region of the resonator, as illustrated in Fig. 4(a). Such a spatially localized modulation $\chi(\mathbf{r}, \omega')$ can then provide the necessary \mathbf{k} components to couple different modes (namely, the overlap integral is non-zero). Eq. (15), together with the relevant overlap integral, also shows that if $\tilde{\chi}(\omega < 0, \omega') = 0$ (spectrally causal), then the modulation will excite only the modes n for which $\omega_n > \omega_m$. Similarly, if $\tilde{\chi}(\omega > 0, \omega') = 0$ (spectrally anti-causal), then only the modes n with $\omega_n < \omega_m$ will be excited. Hence, if the time-varying system is designed to be spectrally causal or anti-causal by suitably pairing a temporal modulation of the refractive index with a modulation of the loss coefficient (no gain is required here), we obtain truly unidirectional “propagation” along the synthetic discrete dimension formed by the frequencies of the modes of the resonator. In addition, such a loss-induced unidirectional propagation is direction-tunable in synthetic space depending on the

causality of the applied modulation. Following this rationale, we designed a temporally modulated ring resonator, and we focused our attention on five of its modes (see middle row of Fig. 4(b) and Methods section). The ring resonator was initially excited at the mode ω_3 and three different cases were investigated (see Methods section for details): (A) Spectrally non-causal, (B) spectrally causal, and (C) spectrally anti-causal. We observe in Fig. 4(b) that in case (A) the modulation excites modes bidirectionally along the frequency axis, whereas in cases (B) and (C) the excitation becomes strictly unidirectional, as expected. We note that the physics underlying this form of unidirectional frequency transport is substantially different from other mechanisms that require, for instance, precise phase detuning [39]. Here, instead, the unidirectional transport stems from the interplay between refractive-index and loss-coefficient modulation, as can also be noted when comparing cases (B) and (C), which have the same loss profile, but create opposite frequency-transport effects due to the different real part of the modulation. An advantage of our method is the fact that the modulation can be applied on demand at any time and does not need to be periodic, hence avoiding any requirement on the precise control of a periodic modulation phase. Thus, the proposed modulation scheme provides direct and flexible control over light propagation along the synthetic frequency dimension, as opposed to periodic modulations that need to be constantly applied and have less flexibility. We, therefore, believe that the proposed modulation strategy, stemming from the concept of spectral causality, might provide a unique tool to observe and enrich various physical phenomena along synthetic dimensions in systems with structurally lower dimensions.

4. CONCLUSIONS

While the scattering properties of spatially varying (inhomogeneous) optical systems have been intensively studied over several decades, wave scattering due to time-varying optical properties has received relatively less attention, especially in the context of non-Hermitian (*i.e.* complex) time modulations. Although a few recent works have shown that the notion of PT-symmetric gratings can be translated into the temporal realm, no general method existed so far to design broader classes of non-Hermitian temporal systems with pre-determined scattering properties. In this regard, we believe that the present work provides relevant tools – the concept of spectral causality and the temporal anti-Kramers-Kronig relations – to extend and generalize temporally modulated (meta)materials to the complex domain. More broadly, by extending the fundamental concept of causality, and its implications, to the spectral domain, our findings may open a new landscape of opportunities to control the scattering of waves beyond what is achievable with conventional static structures and devices. As relevant examples, we have shown that these ideas have direct implications for several applications, such as broadband reflectionless absorption, temporal invisibility and cloaking, and unidirectional frequency translation. Incidentally, we note that this notion of spectral causality for time-varying non-Hermitian materials is mathematically related to the concept of single-sideband modulations in communication systems [41], an analogy that suggests the possibility of further taking inspiration from analog communication systems to design even more advanced time-varying metamaterials.

From a practical standpoint, we also note that, although experimental limitations might hinder the realization of very fast modulations in the optical domain, the proposed concepts can be applied equally well for slowly modulated

metamaterials working at longer operational wavelengths. Most importantly, our findings are general and can be translated to any domain of wave physics, including for acoustics and elastodynamics, which may provide a particularly fertile ground to test some of the ideas proposed in this paper.

METHODS

Full-wave simulations

In this work, causal full-wave simulations have been performed using the finite-difference time-domain method through a commercially available software (Lumerical FDTD Solutions, <https://www.lumerical.com/products/fdtd/>). The time-varying dispersive susceptibility profiles were implemented as custom material plugins by employing the auxiliary differential equation method [40].

In Fig. 2, the input pulse has a center frequency of 530 THz and a bandwidth of 100 THz. The complex susceptibility profile of the medium follows Eq. (9) with the following parameters: $\epsilon_s = 1$, $\omega_0 = 2\pi 500$ THz, $\omega_p = 0.9 \omega_0$, $\gamma = 0.014 \omega_0$, $K = 0.0021 \omega_0^2$, and $t_{\text{offset},1} = -0.14$ ps. In the static case K is set to 0. Both structures are one-dimensional along the x -axis and semi-infinite from $x = 0$ to $x \rightarrow \infty$.

In Fig. 3, the input pulse has a center frequency of 375 THz and a bandwidth of 22 THz. The complex susceptibility profile of the “cloaked” time-varying medium follows Eq. (10) with the following parameters: $\epsilon_s = 1$, $f_1 = -1$, $\omega_0 = 2\pi 500$ THz, $\omega_p = 0.06 \omega_0$, $\gamma = 0.002 \omega_0$, $K = 6.4 \times 10^{-4} \omega_0^2$, $t_{\text{offset},1} = -0.6$ ps, and $t_{\text{offset},2} = -0.7$ ps. The purely Hermitian susceptibility profile of the “uncloaked” time-varying medium follows a lossless Drude dispersion model (with a plasma frequency equal to $\omega_p = 2\pi 3.75$ THz) where the high-frequency limit of the susceptibility is modulated in time to obtain the real susceptibility profile in Fig. 3(b) at 375 THz. Additionally, a global high-frequency susceptibility offset of 2 was added (with the simulation parameters re-scaled accordingly) to avoid any numerical instability arising due to negative susceptibilities. In the spectrally non-causal case (in the animation in Supplementary Material) the parameters are the same as in the cloaked case, except $t_{\text{offset},1} = 0.15$ ps. In all three cases the structure is one-dimensional and spatially-invariant along the x -axis.

In Fig. 4, the electric field magnitude has been recorded at time $t = 1.5$ ps. The ring resonator has an inner and outer radius equal to 0.8 and 1.0 μm , respectively, and a static relative permittivity $\epsilon_s = 3$. The perturbed region subtends an angle of 4° with respect to the origin of the resonator. The frequencies of the modes ω_1 , ω_2 , ω_3 , ω_4 , and ω_5 are equal to 2 π 404 THz, 2 π 429 THz, 2 π 454 THz, 2 π 479 THz, and 2 π 504 THz; respectively. The time-varying complex susceptibility profile of the perturbed region of the ring resonator follows Eq. (9). The parameters for case B are as follows: $\omega_0 = 2\pi 500$ THz, $\omega_p = 0.4 \omega_0$, $\gamma = 0.01 \omega_0$, $K = 6.4 \times 10^{-4} \omega_0^2$, and $t_{\text{offset}} = -0.4$ ps. The parameters for case C are the same as for case B, except $t_{\text{offset}} = 0.7$ ps. On the other hand, the time-varying purely Hermitian susceptibility profile in case A are the same as the real part of the susceptibility profile in case B, except $\omega_p = 0.25 \omega_0$. The purely

Hermitian susceptibility profile has been modeled as a lossless Drude dispersion model (having a plasma frequency equal to $\omega_p = 2\pi 4.54$ THz) with a time-varying high-frequency limit.

ACKNOWLEDGMENTS

The authors acknowledge support from the National Science Foundation (NSF) with Grant No. 1741694, and the Air Force Office of Scientific Research with Grant No. FA9550-19-1-0043. Z.H. also acknowledges support through the Fulbright Foreign Student Program of the U.S. Department of State.

AUTHOR CONTRIBUTIONS

F.M. initiated and supervised the study. Z.H. devised the theory, conceived the applications, proposed the method to realistically implement the concept, carried out the numerical calculations, analyzed the results, prepared the figures and animations, and, together with F.M., wrote the manuscript. All authors contributed to the initial discussions that formed a conceptual basis for the study.

REFERENCES

1. Morgenthaler, F. R. Velocity Modulation of Electromagnetic Waves. *IRE Trans. Microw. Theory Tech.* **6**(2), 167-172 (1958). doi:10.1109/TMTT.1958.1124533
2. Bohren, C. F. *Absorption and scattering of light by small particles* (John Wiley & Sons, 1983). doi:10.1088/0031-9112/35/3/025
3. van de Hulst, H.C. *Light scattering by small particles* (Courier Corporation, 1981).
4. Cassedy, E. S. & Oliner, A. A. Dispersion Relations in Time-Space Periodic Media: Part I—Stable Interactions. *Proceedings of the IEEE* **51**(10), 1342-1359 (1963). doi:10.1109/PROC.1963.2566
5. Felsen, L. B. & Whitman, G. M. Wave Propagation in Time-Varying Media. *IEEE Trans. Antennas Propag.* **18**(2), 242-253 (1970). doi:10.1109/TAP.1970.1139657
6. Kalluri, D. K. & Goteti, V. R. Frequency shifting of electromagnetic radiation by sudden creation of a plasma slab. *J. Appl. Phys.* **72**(10), 4575-4580 (1992). doi:10.1063/1.352111
7. Sounas, D. L. & Alù, A. Non-reciprocal photonics based on time modulation. *Nature Photonics* **11**(12), 774-783 (2017). doi:10.1038/s41566-017-0051-x
8. Tucker, R. S., Ku, P. C. & Chang-Hasnain, C. J. Slow-light optical buffers: Capabilities and fundamental limitations. *J. Light. Technol.* **23**(12), 4046-4066 (2005). doi:10.1109/JLT.2005.853125
9. Ozawa, T. et al. Topological photonics. *Rev. Mod. Phys.* **8**(11), 821-829 (2019). doi:10.1103/RevModPhys.91.015006
10. Hayran, Z., & Monticone, F. Capturing Broadband Light in a Compact Bound State in the Continuum. *arXiv preprint arXiv:2006.03699* (2020).
11. Caloz, C. & Deck-Leger, Z. L. Spacetime Metamaterials-Part II: Theory and Applications. *IEEE Trans. Antennas Propag.* **68**(3), 1583-1598 (2020). doi:10.1109/TAP.2019.2944216

12. Huidobro, P. A., Galiffi, E., Guenneau, S., Craster, R. V. & Pendry, J. B. Fresnel drag in space–time-modulated metamaterials. *Proc. Natl. Acad. Sci.* **116**(50), 24943–24948 (2019). doi:10.1073/pnas.1915027116
13. Galiffi, E. et al. Wood anomalies and surface-wave excitation with a time grating. *Phys. Rev. Lett.* **125**(12), 127403 (2020). doi:10.1103/PhysRevLett.125.127403
14. Koutserimpas, T. T., Alù, A. & Fleury, R. Parametric amplification and bidirectional invisibility in PT - symmetric time-Floquet systems. *Phys. Rev. A* **97**(1), 013839 (2018). doi:10.1103/PhysRevA.97.013839
15. Koutserimpas, T. T. & Fleury, R. Nonreciprocal Gain in Non-Hermitian Time-Floquet Systems. *Phys. Rev. Lett.* **120**(8), 087401 (2018). doi:10.1103/PhysRevLett.120.087401
16. Qin, C., Wang, B., Wong, Z. J., Longhi, S. & Lu, P. Discrete diffraction and Bloch oscillations in non-Hermitian frequency lattices induced by complex photonic gauge fields. *Phys. Rev. B* **101**(6), 064303 (2020). doi:10.1103/PhysRevB.101.064303
17. Xie, Q., Rong, S. & Liu, X. Exceptional points in a time-periodic parity-time-symmetric Rabi model. *Phys. Rev. A* **98**(5), 052122 (2018). doi:10.1103/PhysRevA.98.052122
18. Liu, Q., Qin, C., Wang, B., & Lu, P. Scattering singularities of optical waveguides under complex modulation. *Phys. Rev. A* **101**(3), 033818 (2020). doi:10.1103/PhysRevA.101.033818
19. Miri, M. A. & Alù, A. Exceptional points in optics and photonics. *Science* **363**(6422) (2019). doi:10.1126/science.aar7709
20. Feng, L., El-Ganainy, R. & Ge, L. Non-Hermitian photonics based on parity-time symmetry. *Nature Photonics* **11**(12), 752–762 (2017). doi:10.1038/s41566-017-0031-1
21. Horsley, S. A. R., Artoni, M. & La Rocca, G. C. Spatial Kramers-Kronig relations and the reflection of waves. *Nat. Photonics* **9**(7), 436–439 (2015). doi:10.1038/nphoton.2015.106
22. Longhi, S. Bidirectional invisibility in Kramers–Kronig optical media. *Opt. Lett.* **41**(16), 3727–3730 (2016). doi:10.1364/ol.41.003727
23. Sounas, D. L., Fleury, R. & Alù, A. Unidirectional cloaking based on metasurfaces with balanced loss and gain. *Phys. Rev. Appl.* **4**(1), 014005 (2015). doi:10.1103/PhysRevApplied.4.014005
24. Caloz, C. & Deck-Leger, Z. L. Spacetime Metamaterials-Part I: General Concepts. *IEEE Trans. Antennas Propag.* **68**(3), 1569–1582 (2020). doi:10.1109/TAP.2019.2944225
25. Born, M., & Wolf, E. *Principles of optics: electromagnetic theory of propagation, interference and diffraction of light Ch. XIII.* (Elsevier, 2019).
26. Vezzoli, S. et al. Optical Time Reversal from Time-Dependent Epsilon-Near-Zero Media. *Phys. Rev. Lett.* **120**(4), 043902 (2018). doi:10.1103/PhysRevLett.120.043902
27. Zangwill, A. *Modern electrodynamics Ch. 18* (Cambridge University Press, 2013).
28. García-Meca, C., Ortiz, A. M. & Sáez, R. L. Supersymmetry in the time domain and its applications in optics. *Nat. Commun.* **11**(1), 1–8 (2020). doi:10.1038/s41467-020-14634-0
29. Pacheco-Peña, V. & Engheta, N. Antireflection temporal coatings. *Optica* **7**(4), 323–331 (2020). doi:10.1364/optica.381175
30. Solís D. M., Engheta N. A Generalization of the Kramers-Kronig Relations for Linear Time-Varying Media. *arXiv preprint arXiv:2008.04304* (2020).
31. Stockman, M. I. Nanofocusing of optical energy in tapered plasmonic waveguides. *Phys. Rev. Lett.* **93**(13), 137404 (2004). doi:10.1103/PhysRevLett.93.137404
32. Mann, S. A., Sounas, D. L. & Alù, A. Nonreciprocal cavities and the time-bandwidth limit: reply. *Optica* **7**(9) 1102–1107 (2020). doi:10.1364/optica.401383
33. Gangaraj, S. A. H., Jin, B., Argyropoulos, C. & Monticone, F. Broadband Field Enhancement and Giant Nonlinear Effects in Terminated Unidirectional Plasmonic Waveguides. *Phys. Rev. Applied* **14**(5), 054061 (2020). doi:10.1103/physrevapplied.14.054061
34. Abdelrahman, M. I., Hayran, Z., Chen, A., & Monticone, F. Can fast-light cloaks achieve arbitrarily broadband invisibility?. *arXiv preprint arXiv:2011.02333* (2020).

35. Nistad, B., & Skaar, J. Causality and electromagnetic properties of active media. *Physical Review E* 78(3), 036603 (2008). doi:10.1103/PhysRevE.78.036603
36. Chen, A., & Monticone, F. Active Scattering-Cancellation Cloaking: Broadband Invisibility and Stability Constraints. *IEEE Trans. Antennas Propag.*, **68**(3), 1655-1664 (2019). doi:10.1109/TAP.2019.2948528
37. Ozawa, T., Price, H. M., Goldman, N., Zilberberg, O. & Carusotto, I. Synthetic dimensions in integrated photonics: From optical isolation to four-dimensional quantum Hall physics. *Phys. Rev. A* **93**(4), 043827 (2016). doi:10.1103/PhysRevA.93.043827
38. Srinivasan, K., & Painter, O. Momentum space design of high-Q photonic crystal optical cavities. *Optics Express* **10**(15), 670-684 (2002). doi:10.1103/PhysRevA.93.043827
39. Yuan, L. & Fan, S. Bloch oscillation and unidirectional translation of frequency in a dynamically modulated ring resonator. *Optica* **3**(9), 1014-1018 (2016). doi:10.1364/optica.3.001014
40. Kalluri, D. K. *Electromagnetics of time varying complex media: frequency and polarization transformer Ch. 11* (CRC Press, 2018).
41. Oppenheim, A. V., Willsky, A. S., & Nawab, S. H. *Signals and systems Ch. 8* (Prentice Hall, 1997).

(†) Online link to supplementary movie 1: http://tiny.cc/spect_caus_mov1 and supplementary movie 1: http://tiny.cc/spect_caus_mov2

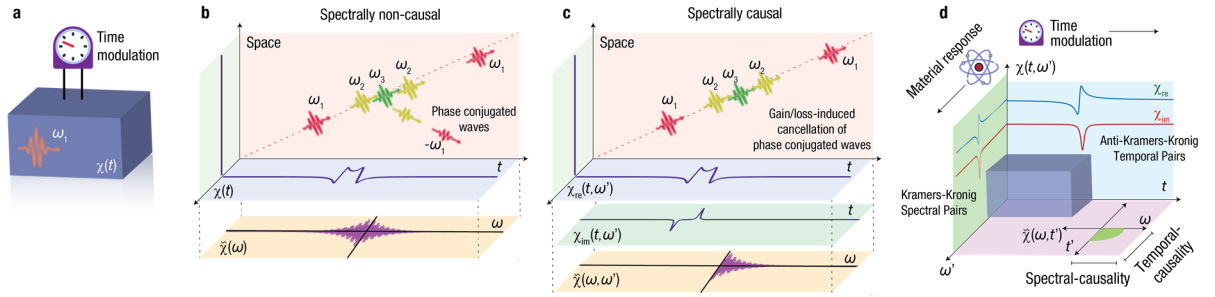


Figure 1 | Spectral causality and its physical implications. **a**, Propagation of a quasi-monochromatic electromagnetic wave within a homogeneous medium whose optical parameters can be controlled dynamically in time. **b**, Upon encountering an arbitrary, real, temporal electric susceptibility perturbation $\chi(t)$, the pulse will experience time-refraction and time-reflection leading to time-shift in the transmitted field and the generation of negative frequencies (phase-conjugated and reflected waves), respectively. Bottom panel: Fourier transform of $\chi(t)$. **c**, A complex susceptibility perturbation, on the other hand, can prevent the generation of any negative frequencies if the real and the imaginary parts of the time-varying electric susceptibility are anti-Kramers-Kronig temporal pairs. Bottom panel: Fourier transform of $\chi(t, \omega')$; the modulation is spectrally causal since $\tilde{\chi}(\omega < 0, \omega') = 0$. **d**, For physical realizability and spectral causality, $\tilde{\chi}(\omega, \omega')$ must be dispersive and satisfy the anti- and conventional Kramers-Kronig relations in the time and frequency domain, respectively, as discussed in the text. Red dotted lines in (b) and (c) denote the propagation trajectory of the incoming wave in the medium in the absence of any time modulation.

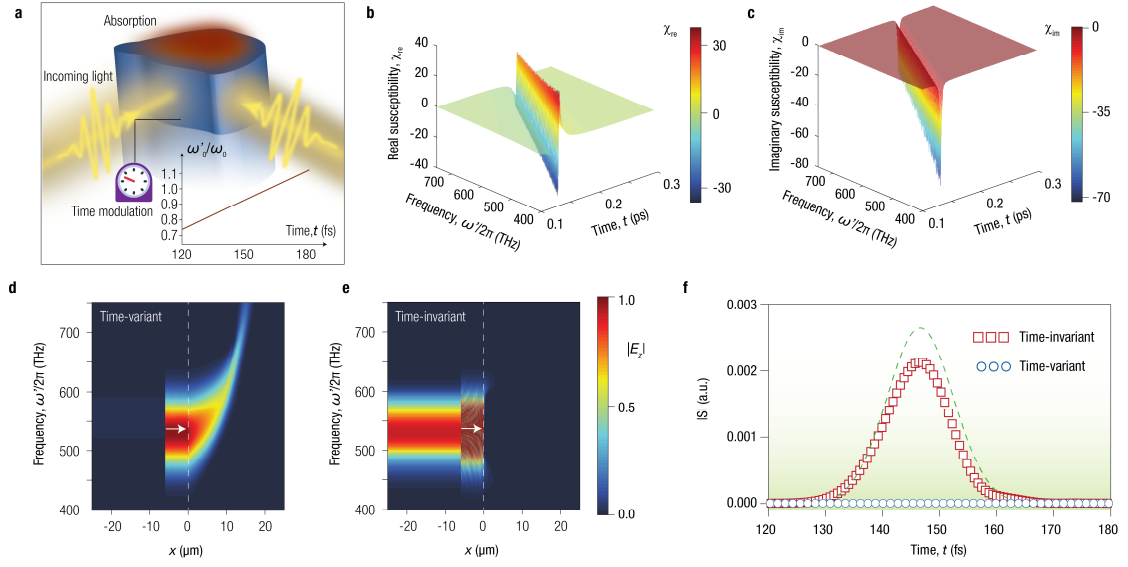


Figure 2 | Broadband reflectionless absorption induced by spectral causality. **a**, The absence of negative frequencies in a spectrally-causal time-scattering process can be exploited to achieve broadband omnidirectional perfect absorption in a lossy medium. The lower right inset shows the modulation of ω_0 in t -time. **b,c**, Real (**b**) and imaginary (**c**) parts of the ω' - frequency-dispersive and t -time-varying electric susceptibility of the designed spectrally (and temporally) causal lossy medium. **d,e**, Spectrally resolved electric field magnitude along the propagation direction for the time modulated (**d**) and static (without time modulation) (**e**) absorbing medium. **f**, Amplitude of the reflected Poynting vector recorded in time at the spatial position $x = -25 \mu\text{m}$. The green dashed line shows the envelope of the instantaneous Poynting vector of the input pulse. In (**d**) and (**e**) white arrows denote the excitation direction, while the white dashed lines mark the interface between free space and the absorbing medium.

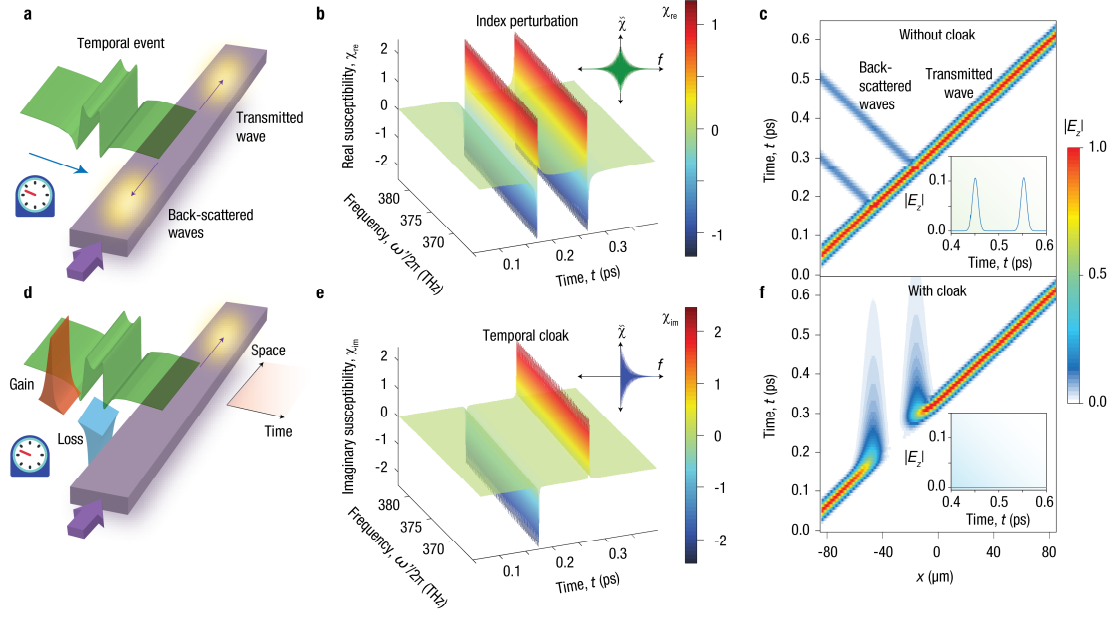


Figure 3 | Temporal cloaking of a refractive-index perturbation via an anti-Kramers-Kronig-pair cloak. **a**, A temporal refractive-index modulation scatters an incident propagating wave, thereby revealing its existence to an observer. **b**, The temporal perturbation consists of a purely Hermitian electric susceptibility modulation (a modulation of the refractive index). **c**, Space-time evolution of a propagating pulse along the propagation direction in the presence of the temporal perturbation. **d,e,f**, A temporal ‘cloak’ consisting of a gain-loss temporal modulation can be designed via the anti-Kramers-Kronig transformation of the refractive-index perturbation (e), as discussed in the text. This effectively renders the perturbation ‘invisible’, hence restoring the propagating wave and suppressing reflections (f). The lower right insets in (c) and (f) show the reflected electric field amplitude at $x = -85 \mu\text{m}$ recorded in time.

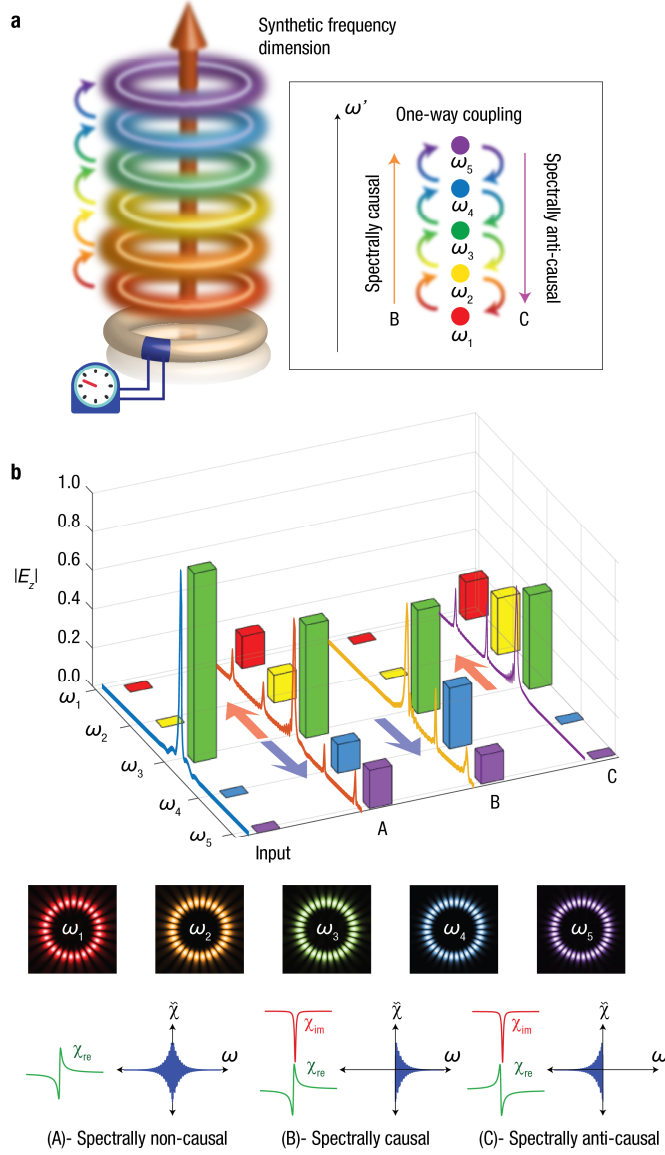


Figure 4 | Loss-induced unidirectional transport along a synthetic dimension. **a**, Temporal modulation of the parameters of a resonant cavity (e.g., a ring resonator) can couple different modes at different frequencies. This creates “propagation” along the ‘synthetic’ dimension formed by the sequence of the frequencies of these resonant modes. The direction of propagation in synthetic space depends on the ‘spectral causality’ of the modulation. **b**, Excited frequency components (resonant modes) for an initially excited mode ω_3

in three different scenarios (see lower row): A- spectrally non-causal Hermitian modulation leading to bidirectional frequency transport, B- spectrally causal modulation leading to unidirectional blue-shifting, C- spectrally anti-causal modulation leading to unidirectional red-shifting. Middle row: Spatial electric field amplitude profiles of the resonator modes. Details about the considered resonator geometry are provided in the Methods section.

Spectral causality and the Scattering of Waves

Supplementary Material

Zeki Hayran, Aobo Chen, Francesco Monticone^{*}

School of Electrical and Computer Engineering, Cornell University, Ithaca, New York 14853, USA

** Corresponding author: francesco.monticone@cornell.edu*

Abstract - This document provides supporting information to the manuscript entitled “Spectral causality and the scattering of waves”.

S1 – Derivation of the Scattering Series

The recursive temporal equation given in Eq. (3) (in the main article) can be reformulated as a scattering series in the frequency domain. By Fourier transforming Eq. (3) (in the main article) and noting that the convolution integral in time domain becomes a multiplication in frequency domain, we obtain

$$\tilde{D} = 2\pi D_0 \delta(\omega - \omega_i) + \tilde{G}(\omega) \left[\left(\tilde{\chi} * (\omega^2 \tilde{D}) \right) (\omega) \right]. \quad (\text{S1})$$

Replacing \tilde{D} on the right-hand side of Eq. (S1) with the full expression of \tilde{D} given by the equation itself yields,

$$\tilde{D} = 2\pi D_0 \delta(\omega - \omega_i) + \tilde{G}(\omega) \left[\left(\tilde{\chi} * \left(\omega^2 \left(2\pi D_0 \delta(\omega - \omega_i) + \tilde{G}(\omega) \left[\left(\tilde{\chi} * (\omega^2 \tilde{D}) \right) (\omega) \right] \right) \right) \right) (\omega) \right], \quad (\text{S2})$$

$$\tilde{D} = 2\pi D_0 \delta(\omega - \omega_i) + 2\pi \omega_i^2 D_0 \tilde{G}(\omega) \left[(\tilde{\chi} * \delta)(\omega - \omega_i) \right] + \tilde{G}(\omega) \left[\tilde{\chi} * \left[\omega^2 \tilde{G}(\omega) \left[\tilde{\chi} * (\omega^2 \tilde{D}) \right] (\omega) \right] \right] (\omega). \quad (\text{S3})$$

The first two terms on the right-hand side of Eq. (S3) correspond to the temporal analogue of the first-order Born approximation in the context of spatial scattering [25]. Such a first-order approximation would be based on a weak-scattering assumption which assumes that the input signal does not undergo a strong perturbation due to its interaction with the medium, and would, therefore, require a very low refractive index contrast (typically on the order of 0.001 [43]). To go beyond such a constraint, we continue the recursive procedure by replacing \tilde{D} on the right-hand side of Eq. (S3) with the full expression of \tilde{D} as in Eq. (S1) to obtain

$$\begin{aligned} \tilde{D} = & 2\pi D_0 \delta(\omega - \omega_i) + 2\pi \omega_i^2 D_0 \tilde{G}(\omega) \left[(\tilde{\chi} * \delta)(\omega - \omega_i) \right] + 2\pi \omega_i^2 D_0 \tilde{G}(\omega) \left[\left(\tilde{\chi} * \left[\omega^2 \tilde{G}(\omega) \left[(\tilde{\chi} * \delta)(\omega - \omega_i) \right] \right) \right) (\omega) \right] \\ & + \tilde{G}(\omega) \left[\left(\tilde{\chi} * \left[\omega^2 \tilde{G}(\omega) \left[\left(\tilde{\chi} * \left[\omega^2 \tilde{G}(\omega) \left[\tilde{\chi} * (\omega^2 \tilde{D}) \right] (\omega) \right] \right) \right] \right) (\omega) \right] \right] (\omega), \end{aligned} \quad (\text{S4})$$

where now the first three terms on the right-hand side of Eq. (S3) can be designated as the second-order *temporal* Born approximation. By repeating similar steps, we obtain the temporal scattering series for any order N as in Eqs. (4-6) in the main article.

S2 – Spectral Profile of the Susceptibility Function

Figure S1(a) shows the $\tilde{\chi}(\omega, \omega')$ spectrum of the susceptibility profile given in Eq. (9) (in the main article), where the causal spectrum (*i.e.* $\tilde{\chi}(\omega < 0, \omega') = 0$) can be clearly observed. Moreover, Fig. S1(b) shows the complex susceptibility temporal variation at a specific ω' . The real and imaginary part of the t -time variation of the susceptibility approximately satisfies the anti-Kramers-Kronig relations, while their ω -spectrum has a nearly causal behavior as seen in Fig. S1(c).

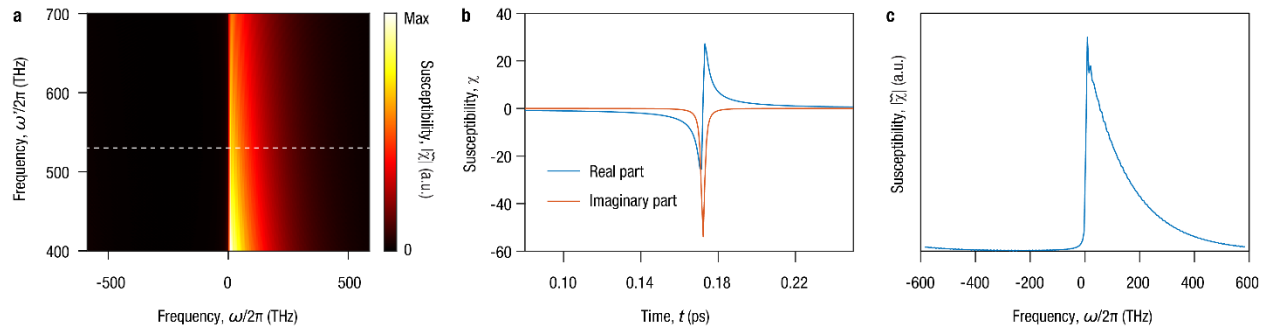


Figure S1 | Susceptibility spectral profile. **a**, The $\tilde{\chi}(\omega, \omega')$ spectrum of the susceptibility profile given in Eq. (9) (in the main article). **b,c**, The temporal variation of the susceptibility profile along the t -axis (**b**) and the magnitude of its Fourier spectrum along the ω -axis (**c**) at $\omega' / 2\pi = 530$ THz (denoted with the white dashed line in (**a**)). The parameters are the same as in Fig. 2 (in the main article).

REFERENCES

42. Born, M., & Wolf, E. *Principles of optics: electromagnetic theory of propagation, interference and diffraction of light Ch. XIII.* (Elsevier, 2019).
43. Gerke, T. D. & Piestun, R. Aperiodic volume optics. *Nat. Photonics* **4**(3), 188-193 (2010).
doi:10.1038/nphoton.2009.290